Numerical modeling of skimming flow over stepped spillways: application on small embankment dams

Inês Sousa Alves Lúcio

Supervisors:
Prof. Dr. Jorge de Saldanha Gonçalves Matos
Prof. Dr. Inês Osório de Castro Meireles

Instituto Superior Técnico, Lisboa, Portugal

December 2015

Abstract

Recently, it has been found that a significant number of embankment dams were unable to meet the hydraulic-operational safety requirements, due to inadequate spillway capacity in extreme flood events. Among the usual rehabilitation measures, roller-compacted concrete (RCC) stepped overlays have gained acceptance for providing overtopping protection during extreme flood events.

The present dissertation presents a numerical study based on simulations performed with the commercial computational fluid dynamics (CFD) code FLOW-3D®. The numerical results are compared with those acquired on an experimental facility representative of a small embankment dam providing for safe overtopping, by means of a 1V:2H sloping stepped chute. FLOW-3D® simulations (2D) were performed for several discharges using the RNG $\kappa - \varepsilon$ turbulence model. The numerical results of flow depths and velocity profiles on the broad-crested weir and stepped chute were validated with available experimental data.

In general, a good agreement between numerical and experimental data was obtained in the broad-crested weir as well as in the stepped chute. However, the precise CFD modeling of the boundary layer and the self-aerated flow region, downstream the inception point, remains a challenge for further research.

Keywords: Embankment dams; stepped spillways; skimming flow; computational fluid dynamics; FLOW-3D®.

1. Introduction

Roller compacted concrete (RCC) stepped overlays have been increasingly used in small embankment dams for providing overtopping protection and increased spillway capacity. The macro-roughness created by the steps induces significant energy dissipation. Hence, it is possible to reduce the size of the downstream energy dissipation structure and minimize the construction costs. The presence of the steps allows the development of the boundary layer to be faster than in smooth, conventional spillways. When the boundary layer reaches the free surface, turbulence induces strong aeration.

For a given chute slope, the flow regime may be either nappe flow at low discharges, transition flow for intermediate discharges or skimming flow at larger discharges (e.g., Essery and Horner, 1978, Diez-Cascon et al., 1991, Elviro and Mateos, 1995, Ohtsu and Yasuda, 1997, Matos, 1999, Fael, 2000, Chanson, 2002, Meireles, 2004). In skimming flows, two different regions are defined: a non-aerated region and an aerated region. Initially, close to the crest, the flow is smooth and glassy and the boundary layer is developing (non-aerated region). When the boundary layer reaches the free-surface, large

quantities of air begin to entrain in the flow (inception point), and flow bulking, splashing and "white waters" are observed (aerated region) (e.g. Chanson, 1994, Matos, 1999, Chanson, 2002, Meireles et al., 2014). In this type of flows, it is possible to distinguish a main flow over the surface tangent to consecutive step edges (pseudo-bottom), and a secondary flow that occupies the cavities formed by the steps. In these cavities, re-circulating vortices are generated.

The aim of this study is the implementation and validation of a numerical model simulating the skimming flow over a stepped spillway, using the commercial CFD code FLOW-3D®. For validation purposes, the numerical results are compared with experimental data previously acquired by other authors.

Recent developments in CFD codes and hardware technology enabled the use of numerical models as a complement to experimental studies for the analysis of flow in stepped spillways. A summary of the main features of previous numerical studies on stepped spillways is presented in Table 1.

Table 1: Summary of the main features of previous numerical studies on stepped spillways.

Author	**Commercial Software**	**Treatment of free-surface**	**Turbulence model**	**Slope** (V.H)	**Number of steps**	**Type of mesh**	**Flow rate** (m^2/s)	**Comparison with data**
Tabbara et al. (2005)	ADINA-F	*Re-meshing*	$k-\varepsilon$	1:0.75	-	Non structured	-	Water depths
Cheng et al. (2006)	FLUENT	MMF	RNG $k-\varepsilon$	1:0.75	13	Non structured	-	Velocities, air entrainment, pressure fields
Arantes (2007)	ANSYS CFX 10.0	Partial VOF	Reynolds stress	1:0.75	-	Non structured	0.0688-0.201	Velocities, water depths
Qian et al. (2009)	-	VOF	Realizable $k-\varepsilon$, SST $k-\omega$, v^2-f, LES	1:0.8	40	-	0.11	Velocities, vorticity, boundary layer
Carvalho and Amador (2008)	-	VOF	-	1:0.8	-	-	0.11	Velocities, turbulence intensities
Bombardelli et al. (2010) Meireles (2011)	FLOW-3D®	TruVOF	$k-\varepsilon$, RNG $k-\varepsilon$	1:0.75	-	Structured	0.08, 0.14, 0.18	Water depths, velocities and boundary layer development
Meireles et al. (2010) Meireles (2011)	FLOW-3D®	TruVOF	RNG $k-\varepsilon$	1:2	10	Structured	0.05, 0.06, 0.07	Water depths, velocities
Kositgittwong (2012)	FLUENT	VOF e MMF	Standard $k-\varepsilon$ Standard $k-\omega$ RNG $k-\varepsilon$ SSR $k-\omega$ Realizable $k-\varepsilon$	1:2	Smooth; 25; 50	Structured	0.47; 0.92 1.38;1.87 2.33	Water depths, velocities, turbulence intensity, energy dissipation
Cheng et al. (2014)	FLUENT	VOF	RNG $k-\varepsilon$	1:6.5 -1:0.75	68; 40, 13	Non structured	0.067- 0.899	Velocities, water depths
Valero and Bung (2015)	FLOW-3D®	TruVOF	RNG $k-\varepsilon$	1:2	23	Structured	0.07 0.09 0.11	Water depths, velocities, air concentrations
Present study	FLOW-3D®	TruVOF	RNG $k-\varepsilon$	1:2	10	Structured	0.05; 0.06 0.07; 0.08	Velocities and water depths in the broad-crested weir and chute spillway

2. Physical model

The numerical model reproduces an experimental facility that was assembled at the Laboratory of Hydraulics and Water Resources at Instituto Superior Técnico (IST), University of Lisbon. The facility comprises a broad-crested weir followed by a stepped chute, and a stilling basin. The broad-crested weir is 0.5 m high, 0.5 m long and 0.7 m wide. The stepped chute is 0.5 m high (from crest to toe), 0.7 m wide, and has a slope of 1V:2H (26.6 degrees from horizontal). The stilling basin is 3.7 m long and 0.7

m wide, and the overshot gate located in its downstream end allows the formation of a hydraulic jump. Experimental results were undertaken in the framework of the Graduate Research Report of André and Ramos (2003) and the MSc thesis of Cabrita (2007) (Table 2). The skimming flow regime occurs for the geometric and flow conditions addressed in those studies, as well as in the numerical simulations carried out in the present research .

Table 2: Summary of the experimental conditions presented in this study.

Author	**Slope** (V:H)	**Step height** (cm)	**No. of steps**	**q** (m^2/s)	**Measurements in the broad-crested weir**	**Measurements in the stepped chute**
André and Ramos (2003)	1:2	5	10	0.05; 0.06 0.07; 0.08	-	Water depths measured along the left wall and velocity profiles
Cabrita (2007)	1:2	5	10	0.05; 0.06 0.07; 0.08	Water depths and velocity profiles	

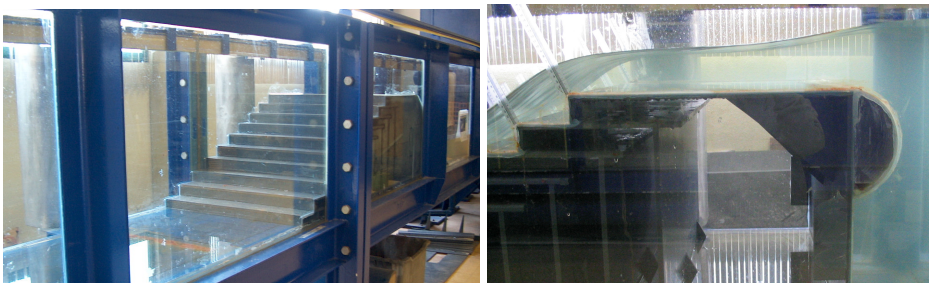

(a) (b)

(c) (d)

Figure 1: Experimental facility: (a) main view; (b) flow over broad-crested weir to Q=49 l/s; (c) step cavity in aerated region of the flow to Q=35l/s; (d) hydraulic jump at the toe of the spillway (André and Ramos, 2003).

3. Mathematical model

The basic equations of a CFD model are the governing equations for fluid dynamics: the continuity equation (conservation of mass), presented in Eq. 1, and the momentum equations, presented in Eq. 2, often referred to as the Navier-Stokes equations (for an incompressible fluid):

$$\frac{\partial u_i}{\partial x_i} = 0 \tag{1}$$

$$\frac{\partial u_i}{\partial t} + u_j \frac{\partial u_i}{\partial x_j} = -\frac{1}{\rho}\frac{\partial p}{\partial x_i} + \nu\left(\frac{\partial^2 u_i}{\partial x_j \partial x_j}\right) + g_i \tag{2}$$

where u_i and u_j are the velocity components in directions x_i and x_j; ρ is the density; p is the pressure;

t is the time coordinate; ν is the kinematic viscosity and g is the gravitational acceleration.

4. Numerical model

FLOW-3D® is a powerful CFD commercial code, developed by FlowScience, Inc., capable of solving a wide range of fluid flow problems (Vanneste, 2012, Fadaei-Kermani and Barani, 2014). It uses the finite volume method to solve the RANS equations (Reynolds Average Navier-Stokes) in a Cartesian, staggered grid. FLOW-3D®uses an advanced algorithm for tracking free-surface flows, TruVOF (developed by Hirt and Nichols, 1981), in which fluid configurations are defined in terms of a VOF function F(x;y;z;t). In one-fluid problems, the air is not treated as a fluid but rather as a void, a region without fluid mass with a uniform reference pressure assigned to it. In this case, F (Fluid Fraction) represents the volume fraction occupied by the fluid: F = 1 in cells completely filled with fluid, and F = 0 in cells with no fluid (void regions) (Flow Science, Inc., 2014, Fadaei-Kermani and Barani, 2014). The free surface is located at a position pertaining to intermediate values of F (usually, where F=0.5, but another intermediate value may be defined by the user) (Bombardelli et al., 2010).

In this software, the operations of geometry building and grid generation are independent of one another: this is called free gridding. Changes in either the grid or geometry can be made freely without requiring changes in the other (Flow Science, Inc., 2015). After both the geometry and the grid are defined, the geometry is then embedded in the computational grid by the preprocessor using a technique called FAVOR™ (Fractional Area/Volume Obstacle Representation) (Flow Science, Inc., 2014). This technique computes the fractional face areas and fractional volumes of the cells that are open to flow and reconstructs the geometry based on these parameters. These ratios are integrated into the governing equations, which results in reformulated equations (for incompressible fluid and no mass sources):

$$\frac{\partial}{\partial x}(uA_x) + \frac{\partial}{\partial y}(vA_y) + \frac{\partial}{\partial z}(wA_z) = 0 \tag{3}$$

$$\frac{\partial u_i}{\partial t} + \frac{1}{V_F}\left[u_j A_j \frac{\partial u_i}{\partial x_j}\right] = -\frac{1}{\rho}\frac{\partial p}{\partial x_i} + G_i + f_i - b_i \tag{4}$$

In these equations, A_x, A_y e A_z are the fractional areas open to flow in x, y e z directions, respectively; V_F is the fractional volume open to flow; G_i are body accelerations; f_i are viscous accelerations; b_i are flow losses in porous media.

5. Numerical model implementation

5.1. Geometry and Mesh

Initially, the solid geometry was imported into FLOW-3D®as an STL file created in AutoCAD. After *FAVORizing* it (*FAVORize* is a tool to assess mesh resolution), it was observed that the cells near the step corners were not well resolved. To avoid possible resolution issues due to this situation, the geometry was generated component by component using the graphical tool for defining geometry available in FLOW-3D ®(Figure 2).

Many computational studies focusing in spillway flow analysis have been carried out in 2D simulations, such as Savage and Johnson (2001), Johnson and Savage (2006), Bombardelli et al. (2010) and

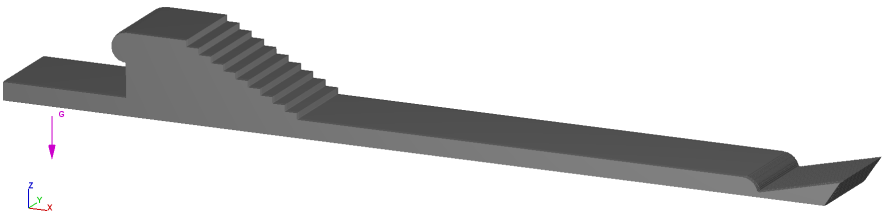

Figure 2: Geometry used in numerical simulations.

Meireles et al. (2010). Although turbulence is a 3D phenomenon, 2D simulations allow to significantly reduce the number of cells in the domain (as well as the computational time) without compromising the results. In this study, 2D simulations were performed. Considering the geometry dimensions and the estimated values of y^+, five different types of meshes were defined (Table 3). A nested block (mesh block defined to be fully within another mesh block, and possibly aligned with the containing block boundaries) was considered in the broad-crested weir and in the stepped chute region: the nested block was designated Block 2 and is represented in Figure 3.

Table 3: Mesh types.

Name	No. of blocks	No. of cells	Cells size (m)
Mesh 1	1	245028	0.0083(3) x 0.0083(3)
Mesh 2	1	431910	0.00625 x 0.00625
Mesh 3	2	436824	Block 1: 0.0083(3) x 0.0083(3) Block 2: 0.004167(7) x 0.004167(7)
Mesh 4	2	735321	Block 1: 0.00625 x 0.00625 Block 2: 0.003125 x 0.003125
Mesh 5	2	1142811	Block 1: 0.005 x 0.005 Block 2: 0.0025 x 0.0025

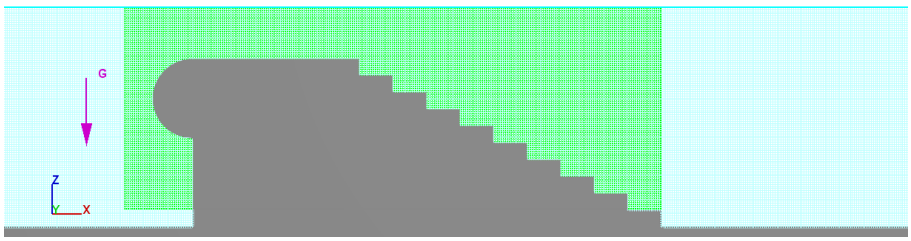

Figure 3: Block 1 (blue) and Block 2 (green).

Aspect ratios of individual cells, between cells and between mesh blocks have been checked and all of them satisfied the recommended neighboring values.

5.2. Boundary conditions

In Block 1, the upstream boundary condition (X_{min}) was defined as Specified Pressure (with definition of the fluid elevation) and the downstream boundary condition (X_{max}) was defined as Outflow. The bottom boundary (Z_{min}) was defined as Wall (no-slip condition) and the top boundary (Z_{max}) was set as Specified Pressure (with Fluid Fraction=0). Both Y_{min} and Y_{max} boundary conditions were set as Symmetry. In Block 2, all boundary conditions were set as Symmetry, except for the Z_{max}, which was defined with the same condition (Specified Pressure) as Block 1 (because the two blocks share this boundary).

5.3. Physical models

The activated physical models were: Gravity, Viscosity and Turbulence, Air Entrainment, Density Evaluation, Drift Flux and Bubble and Phase Change. The chosen turbulence model was RNG $k-\varepsilon$, because in Flow Science, Inc. (2014) is mentioned that RNG $k-\varepsilon$ model has wider applicability than the standard $k-\varepsilon$, and is usually the best choice. Besides, it has been the most used model by other authors in spillway flow analysis (see Table 1). The TLEN (Maximum Turbulent Length Scale) was set to be dynamically computed by the software, after a sensitive analysis on this parameter had been performed. In the Air Entrainment model, bulking and bouyancy options have been activated. In this study, surface tension coefficient was assigned to zero to allow air entrainment, otherwise, no air entrained the spillway. The results pertaining to the non-aerated region were found to be independent of the surface tension coefficient value.

5.4. Mesh independence study

In this study, a mesh independence study has been performed. Relative differences were calculated as $\delta(\%) = \dfrac{V - V_{ref}}{V_{ref}} \cdot 100$, in which V_{ref} refers to the most refined mesh. In the broad-crested weir, the relative differences between mesh 4 and 5 are, in average, 0.2%. In the non-aerated region of the stepped chute, the relative differences are, in average, 0.8%. It was observed that the more refined the mesh is, more air is entrained into the spillway, leading to an increase of the relative differences in the aerated region of the spillway. In the non-aerated region of the spillway, a grid-independent solution has been achieved. In the aerated region, the results were found to be sensitive to the mesh size.

6. Results

This chapter presents a comparison between experimental and numerical results. The simulations performed in this study are summarized in Table 4.

Table 4: Summary of simulations.

Q (l/s)	q (m^2/s)	h_c/h_d	Mesh types	TLEN	Computational time until steady-state
35	0.05	1.27	1 2 3 4 5	Dynamically computed	1h:47m:15s 05h:03:59s 03h:44min:26s 08h:42m:39s 1day:7h:43m:09s
42	0.06	1.43	4 5	Dynamically computed, TLEN=0.004, TLEN=0.006 TLEN=0.008, TLEN=0.01, TLEN=0.02 Dynamically computed	12h:12min, 7h:7min, 7h:39min 9h:30min, 9h:20min, 9h:35min 1day:03h:21m:21s
49	0.07	1.59	1 2 3 4 5	Dynamically computed	1h:45min:27s 03h:30m:56s 04h:18m:25s 10h:15m:16s 1day:2h:24m:48s
56	0.08	1.74	3 4	Dynamically computed	5h:31m:11s 14h:55min:07s

In this section, the relative difference between experimental and numerical results is given by $\delta = \dfrac{V_{num} - V_{exp}}{V_{exp}} \cdot 100$.

6.1. Flow rate (discharge)

In order to verify that the model provided an accurate discharge, velocities in several cross sections of the spillway were integrated numerically, using the trapezoidal rule. Relative differences between experimental and numerical values of discharge in the broad-crested weir and in the stepped chute were, in average, 2.5% and 3.2%, respectively.

Table 5 presents the following relative differences: δ_1 refers to the relative difference between the experimental flow rate, q_{exp}, and the simulated flow rate in the upstream boundary, q_{num} (X_{min}) for t=100s; δ_2 refers to the relative difference between the experimental flow rate, q_{exp}, and the simulated flow rate in the downstream boundary, q_{num} (X_{max}) for t=100s.

Table 5: Relative differences between experimental and numerical values of discharge in X_{min} and X_{max} boundaries (mesh 4).

Q_{exp} (l/s)	q_{exp} (m^2/s)	q_{num} (X_{min}) (m^2/s)	q_{num} (X_{max}) (m^2/s)	δ_1 (%)	δ_2 (%)
35	0.05	0.0484	0.0463	-3.1	-7.4
42	0.06	0.0601	0.0589	0.2	-1.8
49	0.07	0.0686	0.0654	-2.1	-6.6
56	0.08	0.0768	0.0762	-4.1	-4.7

6.2. Broad-crested weir

Figure 4 presents the experimental and numerical water depths in broad-crested weir and Table 6 presents the relative differences between them.

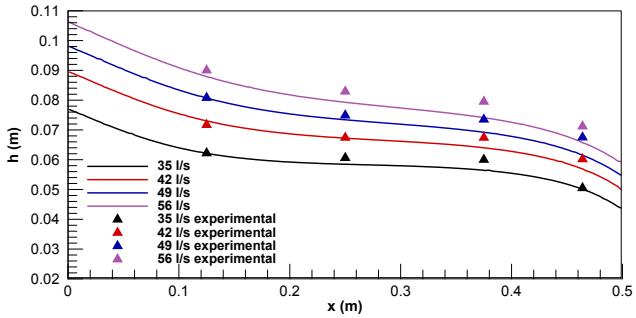

Figure 4: Experimental and numerical water depths along the broad-crest weir.

Table 6: Relative differences between experimental and numerical water depths in the broad-crested weir: (a) Q=35 l/s and mesh 4; (b) Q=42 l/s and mesh 4; (c) Q=49 l/s and mesh 4; (d) Q=56 l/s and mesh 4.

(a)

x	h_{exp} (m)	h_{num} (m)	δ (%)
Section 1	0.0622	0.0621	-0.1
Section 2	0.0606	0.0585	-3.5
Section 3	0.0600	0.0564	-5.9
Section 4	0.0505	0.0501	-0.9

(b)

x	h_{exp} (m)	h_{num} (m)	δ (%)
Section 1	0.0717	0.0730	1.9
Section 2	0.0674	0.0672	-0.2
Section 3	0.0674	0.0640	-5.0
Section 4	0.0602	0.0569	-5.4

(c)

x	h_{exp} (m)	h_{num} (m)	δ (%)
Section 1	0.0808	0.0807	-0.1
Section 2	0.0749	0.0734	-2.0
Section 3	0.0735	0.0692	-5.8
Section 4	0.0675	0.0615	-8.9

(d)

x	h_{exp} (m)	h_{num} (m)	δ (%)
Section 1	0.0900	0.0879	-2.3
Section 2	0.0829	0.0793	-4.4
Section 3	0.0795	0.0741	-6.8
Section 4	0.0712	0.0657	-7.7

The experimental velocities have been compared with numerical velocities for four sections of the broad-crested weir. In sections 1, 2, 3 and 4, the mean relative differences were respectively equal to: 7.5, 5.9, 3.2, and 2.6%, for Q=35 l/s; 10.2, 7.0, 3.3, and 4.7%, for Q=42 l/s; 6.3, 5.3, 2.6, and 7.3%, for Q=49 l/s; and 5.1, 4.4, 2.8, and 8.6%, for Q=56 l/s.

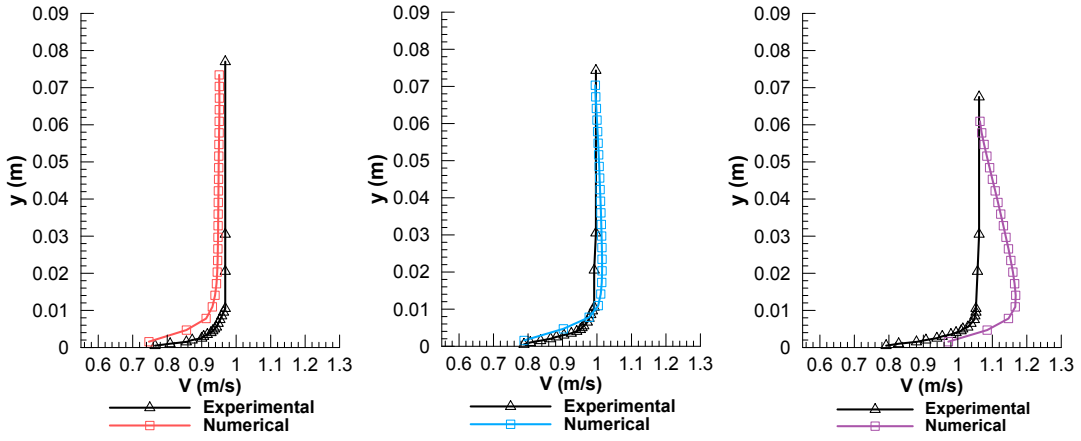

Figure 5: Experimental and numerical velocities in the broad-crested weir (Q=49 l/s and mesh 4): (a) section 2; (b) section 3; (c) section 4.

6.3. Stepped spillway

Fig. 6 presents the experimental and numerical water depths in the stepped spillway.

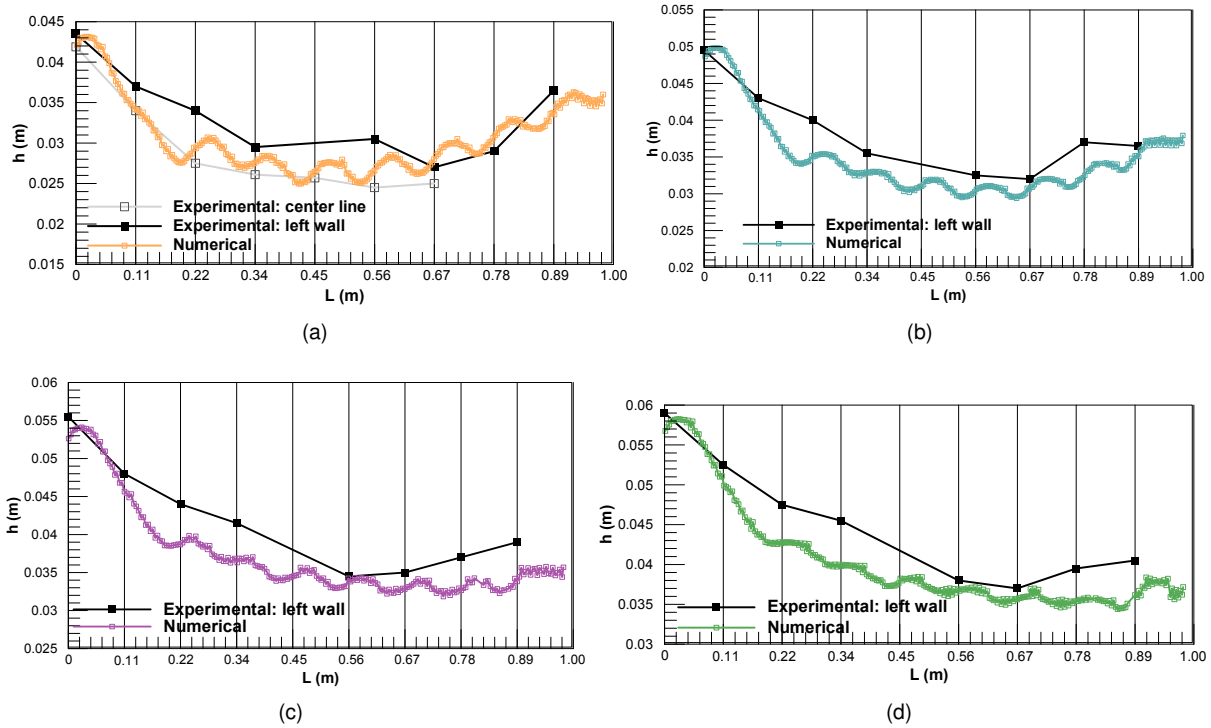

Figure 6: Experimental and numerical water depths along the stepped spillway: (a) Q=35 l/s and mesh 5; (b) Q=42 l/s and mesh 5; (c) Q=49 l/s and mesh 5; (d) Q=56 l/s and mesh 4 (The verticals 1 to 10 correspond to the normal gridlines indicated in the figures, where L varies from 0 to 1.0).

Relative differences between experimental and numerical water depths are presented in Table 7. Therein δ_1 is the relative difference between the water depths measured in the center line of the spillway, $h_{center\ line}$ (only available to Q=35 l/s), and the numerical water depth, h_{num}; δ_2 is the relative difference between the water depth measured in the left wall of the spillway, $h_{left\ wall}$, and the numerical water depth, h_{num}.

Table 7: Relative differences between experimental and numerical water depths: (a) Q=35 l/s; (b) Q=42 l/s; (c) Q=49 l/s; (d) Q=56 l/s.

(a)

Vertical	L (m)	h_{axis} (m)	$h_{left\ wall}$ (m)	h_{num} (m)	δ_1 (%)	δ_2 (%)
1	0.00	0.042	0.044	0.042	0.5	-3.2
2	0.11	0.034	0.037	0.034	0.4	-7.7
3	0.22	0.028	0.034	0.029	6.8	-13.6
4	0.34	0.026	0.030	0.028	5.7	-6.5
5	0.45	0.026	-	0.026	2.9	-
6	0.56	0.025	0.031	0.027	8.6	-12.8
7	0.67	0.025	0.027	0.028	12.2	3.9
8	0.78	-	0.029	0.031	-	6.1
9	0.89	-	0.037	0.034	-	-7.9

(b)

Vertical	L (m)	$h_{left\ wall}$ (m)	h_{num} (m)	δ_2 (%)
1	0.00	0.0495	0.049	-1.7
2	0.11	0.0430	0.041	-3.8
3	0.22	0.0400	0.035	-12.2
4	0.34	0.0355	0.033	-7.2
5	0.45	-	-	-
6	0.56	0.0325	0.030	-6.3
7	0.67	0.0320	0.031	-4.0
8	0.78	0.0370	0.032	-12.5
9	0.89	0.0370	0.035	-3.9

(c)

Vertical	L (m)	$h_{left\ wall}$ (m)	h_{num} (m)	δ_2 (%)
1	0.00	0.0555	0.053	-5.2
2	0.11	0.0480	0.046	-4.9
3	0.22	0.0440	0.039	-12.0
4	0.34	0.0415	0.036	-12.2
5	0.45	-	-	-
6	0.56	0.0345	0.034	-1.1
7	0.67	0.0350	0.033	-6.2
8	0.78	0.0370	0.033	-11.6
9	0.89	0.0390	0.034	-13.2

(d)

Vertical	L (m)	$h_{left\ wall}$ (m)	h_{num} (m)	δ_2 (%)
1	0.00	0.0590	0.057	-3.8
2	0.11	0.0525	0.050	-4.1
3	0.22	0.0475	0.043	-10.1
4	0.34	0.0455	0.040	-12.5
5	0.45	-	-	-
6	0.56	0.0380	0.037	-3.1
7	0.67	0.0370	0.036	-3.7
8	0.78	0.0395	0.035	-10.4
9	0.89	0.0405	0.036	-10.7

The numerical simulations of water depths in the stepped spillway show the wavy pattern of the free-surface. Water depths increase with the flow rate and the amplitude of the free-surface undulation decreases with the flow rate. The increase of the water depths near the downstream end of the spillway (more significant for lower discharges) is due to air entrainment in such flow region (Figure 7).

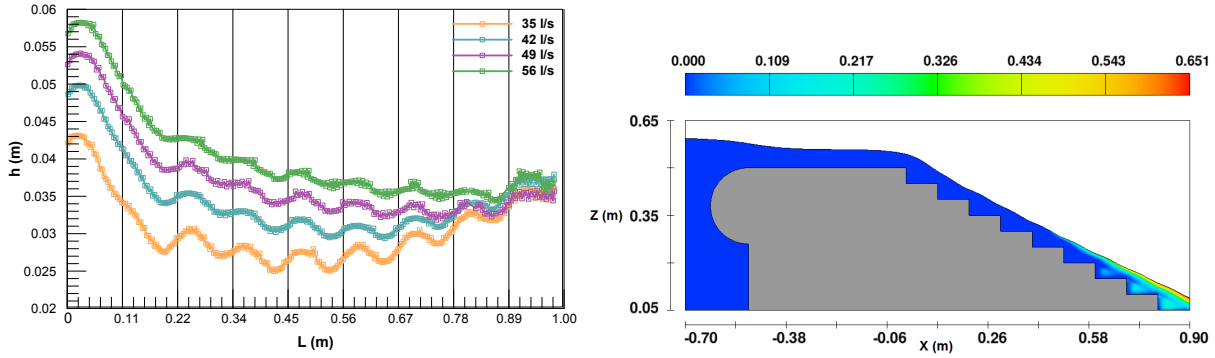

(a) (b)

Figure 7: Flow properties along the stepped spillway obtained from the numerical simulations: (a) numerical flow depths in the stepped spillway; (b) volume fraction of air entrainment to Q=35 l/s and mesh 5.

The experimental velocities have been compared with numerical velocities for six verticals of the stepped spillway. In verticals 2, 3, 4, 5, 6 and 7, the mean relative differences were respectively equal to: 10.5, 14.8, 13.4, 18.4, 12.2 and 14.3%, for Q=35 l/s; 7.8, 14.5, 12.8, 20.0, 16.7 and 14%, for Q=42 l/s.

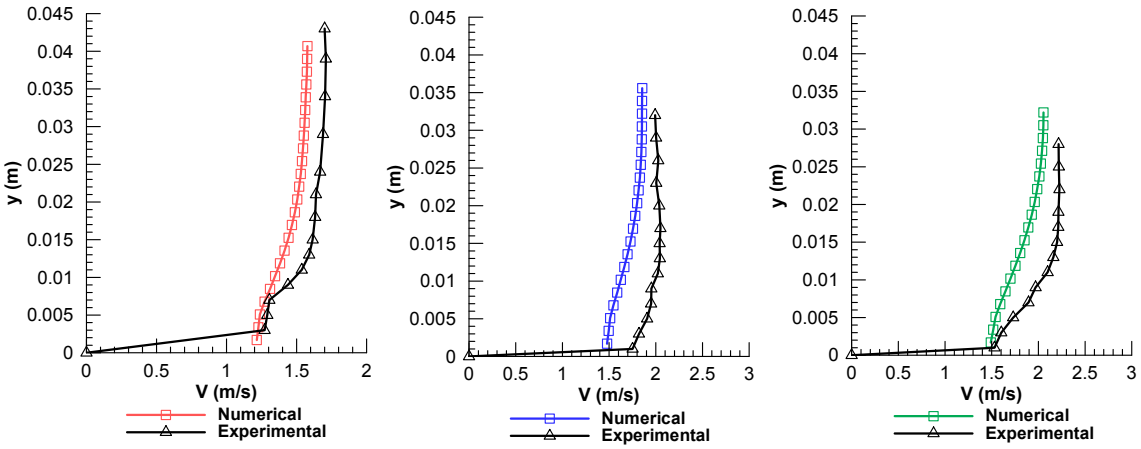

Figure 8: Experimental and numerical velocity profiles in 3 verticals of the stepped spillway (Q=42 l/s and mesh 5): (a) vertical 2; (b) vertical 3; (c) vertical 4.

7. Conclusions

In typical spillways over small embankment dams, the skimming, non-aerated region of the flow is of particular importance for their hydraulic design.

A good agreement between simulated and measured results have been achieved. In the broad-crested weir, the relative differences between experimental and numerical water depths were less than 8.9% (average difference of 3.8%), and the relative differences between experimental and numerical velocities were less than 10.2% (average difference of 5.4%). In the stepped spillway, the relative differences between experimental and numerical water depths were less than 13.6% (average difference of 7.4%), and the relative differences between experimental and numerical velocities were less than 20.0% (average difference of 14.3%). The validation confirms that FLOW-3D® is able to simulate, in general with good accuracy, the flow rate, water depths and velocity distribution of the skimming flow in the non-aerated region of the spillway.

The qualitative study of the inception point of air entrainment has also been one of the focus of the present study. Simulations performed with the abcense of surface tension showed a satisfactory prediction of the inception point of air entrainment, according to visual observations presented in the experimental studies. The need to not account for the surface tension coefficient in order to allow air entrainment in the stepped spillway may be related to some issues in FLOW-3D®air entrainment algorithm (also reported in Bombardelli, 2012) and in boundary layer development (Burnham, 2011), as well as to the fact that 2D simulations do not reproduce 3D effects of a turbulent flow. The values of air concentrations are very sensitive to mesh sizes. Further investigations on boundary layer development and aerated flow region should be considered in future research.

References

André, M. and Ramos, P. (2003). Hidráulica de descarregadores de cheia em degraus e aplicação a descarregadores com paredes convergentes. Graduate Research Report, Instituto Superior Técnico, Lisbon.

Arantes, E. J. (2007). Caracterização do escoamento sobre vertedouros em degraus via CFD. Ph.D. Thesis, EESC USP, São Paulo, Brazil.

Bombardelli, F. (2012). Computational multi-phase fluid dynamics to address flows past hydraulic structures. 4th IAHR International Symposium on Hydraulic Structures, 9-11 February 2012, Porto, Portugal.

Bombardelli, F. A., Meireles, I., and Matos, J. (2010). Laboratory measurements and multi-block numerical simulations of the mean flow and turbulence in the non-aerated skimming flow region of steep stepped spillways. *Environmental Fluid Mechanics*, 10(4):263–288.

Burnham, J. (2011). Modeling dams with computational fluid dynamics: past success and new directions. Dam Safety 2011, National Harbor MD, September, 25-29.

Cabrita, J. (2007). Caracterização do escoamento deslizante sobre turbilhões em descarregadores de cheias em degraus com paredes convergentes. MSc thesis, Instituto Superior Técnico, Lisbon, Portugal.

Carvalho, R. F. and Amador, A. T. (2008). Physical and numerical investigation of the skimming flow over a stepped spillway. Proc. 3rd IAHR Int. Symposium on Hydraulic Structures, Nanjing, China, pp. 1767-1772.

Chanson, H. (1994). Hydraulic Design of Stepped Cascades, Channels, Weirs and Spillways. Pergamon, Oxford, UK.

Chanson, H. (2002). The Hydraulics of Stepped Chutes and Spillways. Balkema, The Netherlands.

Cheng, X., Chen, Y., and Luo, L. (2006). Numerical simulation of air-water two-phase flow over stepped spillway. *Science in China Series E: Technological Sciences*, 49(6):674–684.

Cheng, X., Gulliver, J. S., and Zhu, D. (2014). Application of displacement height and surface roughness length to determination boundary layer development length over stepped spillway. *Water 2014*, (6):3888–3912.

Diez-Cascon, J., Blanco, J. L., Revilla, J., and Garcia, R. (1991). Studies on the hydraulic behaviour of stepped spillways. *Water Power and Dam Construction*, September, pp. 22-26.

Elviro, V. and Mateos, C. (1995). Spanish research into stepped spillways. *The International Jornal on Hydropower and Dams*, September, pp. 61-65.

Essery, I. T. S. and Horner, M. W. (1978). The Hydraulic Design of Stepped Spillways. CIRIA Report no. 33, London, UK.

Fadaei-Kermani, E. and Barani, G. A. (2014). Numerical simulation of flow over spillway based on the cfd method. *Scientia Iranica*, 21(1):91–97.

Fael, C. (2000). Escoamento em quedas sucessivas: ocorrência e dissipação de energia. MSc thesis, Instituto Superior Técnico, Lisbon, Portugal.

Flow Science, Inc. (2014). FLOW-3D User Manual. Version 11.0.3, Santa Fe, New Mexico, USA.

Flow Science, Inc. (2015). FLOW-3D Website. `wwww.flow3d.com`.

Hirt, C. W. and Nichols, B. D. (1981). Volume of Fluid (VOF) method for the dynamics of free boundaries. *Journal of Computational Physics*, 39:201–225.

Johnson, M. C. and Savage, B. (2006). Physical and numerical comparison of flow over ogee spillway in the presence of tailwater. *Journal of Hydraulic Engineering*, 132(12):1353–1357.

Kositgittwong, D. (2012). Validation on numerical model of the flow behaviour through smooth and stepped spillways using large-scale physical model. PhD thesis, King Mongkut's University of Technology Thonburi.

Matos, J. (1999). Emulsionamento de ar e dissipação de energia do escoamento em descarregadores em degraus. PhD Thesis, Instituto Superior Técnico, Lisbon, Portugal.

Meireles, I. (2004). Caracterização do escoamento deslizante sobre turbilhões e energia específica residual em descarregadores de cheias em degraus. MSc thesis, Instituto Superior Técnico, Lisbon.

Meireles, I. (2011). Hidráulica dos descarregadores em degraus: estudo experimental-numérico-teórico. PhD thesis, Universidade de Aveiro, Aveiro.

Meireles, I., Bombardelli, F., and Matos, J. (2010). Experimental and numerical investigation of the non-aerated skimming flow over stepped spillways over embankment dams. 1st European IAHR Congress, Edinburgh, Scotland.

Meireles, I., Bombardelli, F., and Matos, J. (2014). Air entrainment onset in skimming flows on steep stepped spillways: an analysis. *Journal of Hydraulic Research*, 52(3):375–385.

Ohtsu, I. and Yasuda, Y. (1997). Characteristics of flow conditions on stepped channels. Proc. 27th IAHR Congress, Theme D, pp. 583-588, San Francisco, USA.

Qian, Z., Hu, X., Huai, W., and Amador, A. (2009). Numerical simulation and analysis of water flow over stepped spillways. *Science in China Series E: Technological Sciences*, 52(7):1958–1965.

Savage, B. M. and Johnson, M. C. (2001). Flow over ogee spillway: Physical and numerical model case study. *Journal of Hydraulic Engineering*, 127(8):640–649.

Tabbara, M., Chatila, J., and Awwad, R. (2005). Computational simulation of flow over stepped spillway. *Computers and Structures*, 83:2215–2224.

Valero, D. and Bung, D. (2015). Hybrid investigation of air transport processes in moderately sloped stepped spillway flows. E-proceedings of the 36th IARH World Congress, 28 June-3 July, The Netherlands.

Vanneste, D. (2012). *Experimental and numerical study of wave-induced porous flow in rubble-mound breakwaters*, chapter 5. Ghent University.